*minerals*

MDPI

*Article*

# Digital Rock Physics in Cuttings Using High-Resolution Thin Section Scan Images

**Miguel Ángel Caja [1,*], José Nicolás Castillo [1], Carlos Alberto Santos [1], José Luis Pérez-Jiménez [1], Pedro Ramón Fernández-Díaz [1], Vanesa Blázquez [1], Sergi Esteve [2], José Rafael Campos [2], Telm Bover-Arnal [2] and Juan Diego Martín-Martín [2]**

[1] Repsol Technology Lab, C/Agustin de Betancourt, s/n, Móstoles, 28935 Madrid, Spain; josenicolas.castillo@repsol.com (J.N.C.); carlosalberto.santos@repsol.com (C.A.S.); joseluis.perez@repsol.com (J.L.P.-J.); pedroramon.fernandez@repsol.com (P.R.F.-D.); vanesa.blazquez@repsol.com (V.B.)

[2] Department of Mineralogy, Petrology and Applied Geology, University of Barcelona, Martí i Franquès, s/n, 08028 Barcelona, Spain; sergi.esteve@ub.edu (S.E.); joser.campost@gmail.com (J.R.C.); telm.boverarnal@ub.edu (T.B.-A.); juandiegomartin@ub.edu (J.D.M.-M.)

* Correspondence: miguelangel.caja@repsol.com

**Abstract:** Digital rock physics (DRP) has undergone significant advancements in the use of various imaging techniques to acquire three-dimensional volumes and images of rock samples for the computation of petrophysical properties. This study focuses on developing a DRP workflow using high-resolution thin section scans for computing porosity and permeability in cuttings samples. The workflow was tested on quarry sandstone plug samples and artificially generated pseudo-cuttings before applying it to real cuttings from oil and gas wells. The results show that the porosity and permeability values obtained through the DRP workflow are statistically equivalent to those obtained through conventional routine core analysis (RCAL). The workflow was also able to handle the presence of various lithologies in real cuttings samples. The study demonstrates the feasibility of obtaining porosity and permeability values in cutting samples using the DRP approach, offering a fast and cost-effective methodology that provides additional data and allows linking petrophysical properties to image data from the cuttings.

**Keywords:** digital rock physics; thin sections; cuttings; pseudo-cuttings; plugs; routine core analysis

check for updates

**Citation:** Caja, M.Á.; Castillo, J.N.; Santos, C.A.; Pérez-Jiménez, J.L.; Fernández-Díaz, P.R.; Blázquez, V.; Esteve, S.; Campos, J.R.; Bover-Arnal, T.; Martín-Martín, J.D. Digital Rock Physics in Cuttings Using High-Resolution Thin Section Scan Images. *Minerals* **2023**, *13*, 1140. https://doi.org/10.3390/min13091140

Academic Editor: Samintha Perera

Received: 7 June 2023
Revised: 14 July 2023
Accepted: 9 August 2023
Published: 29 August 2023

**Copyright:** © 2023 by the authors. Licensee MDPI, Basel, Switzerland. This article is an open access article distributed under the terms and conditions of the Creative Commons Attribution (CC BY) license (https://creativecommons.org/licenses/by/4.0/).

## 1. Introduction

Oil and gas exploration and development require reservoir characterization, which involves transforming remotely measured properties from geophysical and logging techniques into laboratory experiments to confirm the properties' value in real subsurface rock samples, thereby reducing uncertainty. However, traditional laboratory analysis necessitates intact and perfectly cylindrical rock samples, commonly known as plugs, which can be challenging or costly to obtain for exploration activities [1].

Digital rock physics (DRP) has emerged as a valuable tool for reservoir characterization over the past three decades. It utilizes non-destructive methods to determine petrophysical properties. X-ray computed tomography (CT) or micro-computed tomography (micro-CT) are widely used to create three-dimensional (3D) rock volumes, serving as digital replicas of the materials under investigation [2–6]. These 3D volumes are typically employed for porosity computation through segmentation and for numerical simulations of permeability using the lattice Boltzmann method, which requires powerful and expensive high-performance computing clusters [7–9]. In parallel, scanning electron microscopy (SEM) has demonstrated that not only 3D volumes but also 2D images can serve as supplementary aids to the 3D data [2,3,7,10]. SEM has also enabled the use of thin sections, which are prepared from rocks (plugs, cuttings) and do not possess a cylindrical shape, making them more suitable

for CT and micro-CT analysis. To address this, some researchers have explored confocal laser scan microscopy (CLSM) on thin sections, where epoxy resin impregnating the pores is combined with a chemical additive that activates during laser scanning, enabling visualization of pore space and computation of properties [11–16]. Recent advancements in automatic thin section scanners have further facilitated the application of DRP workflows by providing high-resolution images of entire rock samples in a shorter time and at a relatively lower cost [17]. The algorithms used in DRP approaches often focus on image segmentation, which is performed after image acquisition to compute the petrophysical properties and is referred to as "petrographic image analysis" [13,18–21]. Although previous studies have applied digital approaches to cutting samples, the emphasis has primarily been on mineralogy and lithological identification [3,22–24].

The objective of this study is to develop a DRP workflow for analyzing cutting samples to obtain porosity and permeability using thin sections and a digital approach. The developed method will be initially applied to quarry sandstone plug samples and pseudo-cuttings artificially generated from these plugs for testing purposes. The workflow will be evaluated before its application to real cuttings obtained from oil and gas wells.

## 2. Materials and Methods

### *2.1. Plug Samples*

Plug samples of sandstone were obtained from quarries and provided by Kocurek Industries Inc. These samples had a diameter of 1.5 inches and a length of 3 inches (Figure 1). A total of 7 rock types of sandstone were selected for their homogeneous composition, texture, variety of porosity, and permeability properties. Priority was given to including low, medium, and high permeability values (Table 1). However, one of the samples, Bandera Brown, was reported to have non-homogeneous composition and texture. This particular sample will help us understand how the heterogeneity of the sample affects the obtained petrophysical values.

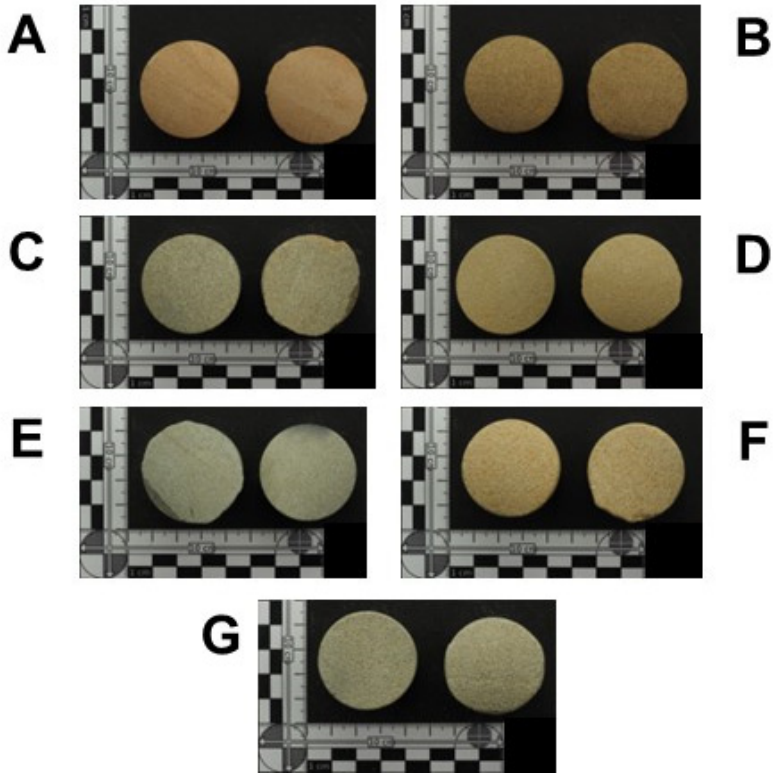


**Figure 1.** Photographs of plug samples: Torrey Buff (**A**), Bandera Brown (**B**), Carbon Tan (**C**), San Saba (**D**), Berea Spider (**E**), Salt Wash North (**F**), and Castlegate (**G**).

**Table 1.** Plug sandstone samples from quarries with low, medium, and high porosity and permeability values.

| ID | Sample ID | Name | Formation | Homogeneous | Porosity (%) | Permeability (mD) |
|---|---|---|---|---|---|---|
| 1 | SS-123 | Torrey Buff | Eocene | Yes | 13–17 | 0.4–3 |
| 2 | SS-100 | Bandera Brown | Desmoinesian | No | 21–23 | 30–45 |
| 3 | SS-109 | Carbon Tan | Late Cretaceous | Yes | 12–17 | 40–50 |
| 4 | SS-121 | San Saba | Paleozoic | Yes | 19–21 | 70–85 |
| 5 | SS-106 | Berea Spider | Upper Devonian | Yes | 19–21 | 120–300 |
| 6 | SS-120 | Salt Wash North | N/A | Yes | 20–22 | 440–800 |
| 7 | SS-110 | Castlegate | Late Cretaceous | Yes | 27–29 | 800–1200 |

### *2.2. Routine Core Analysis in Plug Samples*

Routine core analysis, specifically helium porosity and gas permeability measurements, were conducted on a Coretest system using the AP-608 Automated Permeameter–Porosimeter. The helium expansion method based on Boyle's law was employed to determine pore volume. Permeability was measured using helium, and both porosity and permeability were measured five times for each sample under 500 psi of confining pressure. The instrument consists of a sealed reference chamber filled with Helium gas at room temperature to a pressure of 200 psi. The sample is placed in a sealed chamber connected to the reference chamber through a two-way valve. Opening the valve allows the gas in the reference chamber to expand into the combined volume of the two chambers. By applying Boyle's law and knowing the volume of the reference chamber, initial pressure, and final pressure, the volume of the sample chamber can be calculated. The porosity and grain density of the sample were determined by calculating the bulk volume and weight of the plug. As a quality check, a set of standard samples was run at the beginning of each batch of samples. Each plug was loaded into a hydrostatic core holder, and the necessary overburden was applied. The samples were allowed to reach equilibrium under each confining stress before measurements were taken. Sample pore volumes were directly measured by injecting helium. In this case, the confining pressure was set to the routine value of 500 psi. Following porosity measurements, gas permeability measurements were conducted on the same samples at 500 psi of confining pressure. Helium gas, instead of nitrogen, was used since the samples had a permeability higher than 0.1 mD. The gas was flowed through each sample, and the flow was allowed to stabilize before taking readings. The differential pressure across the sample was measured, and a pulsed decay method under unsteady state conditions was used to calculate permeability. To ensure accurate measurements from the AP-608, an automatic leak check was periodically performed to detect and identify any leaks before and after the measurements. This routine served as a quality control measure for the obtained data. Each plug sample underwent a total of 5 measurements, providing repetition for the test (see Supplementary Materials Table S1).

### *2.3. Pseudo-Cuttings Generation*

Pseudo-cuttings, or artificial cuttings, were generated from the plug samples (Figure 2). Since there is no standardized procedure for particle size analysis of cuttings from well drilling, the ASTM D422 standard test method for particle-size analysis of soils [25] was employed. A FRITSCH jaw crusher was used to obtain 30 g of each sample, resulting in particle sizes ranging between 0.85 and 2.8 mm, which corresponds to the 7/20 fraction according to the ASTM norm (Figure 3). The selection of this size fraction was based on the relationship between the rate of bit penetration (ROP), weight on bit (WOB), and the size of cuttings produced during drilling [26].

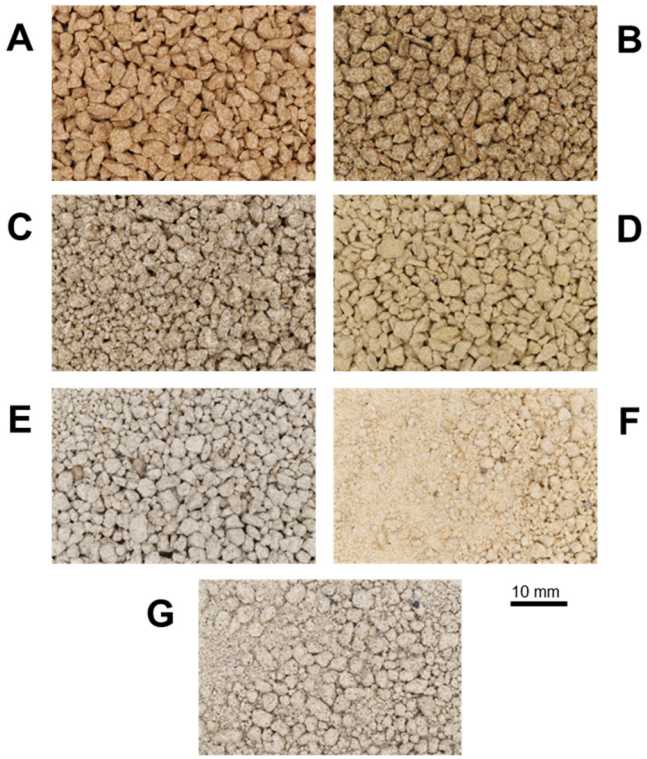


**Figure 2.** Photographs of pseudo-cuttings: Torrey Buff (**A**), Bandera Brown (**B**), Carbon Tan (**C**), San Saba (**D**), Berea Spider (**E**), Salt Wash North (**F**), and Castlegate (**G**).

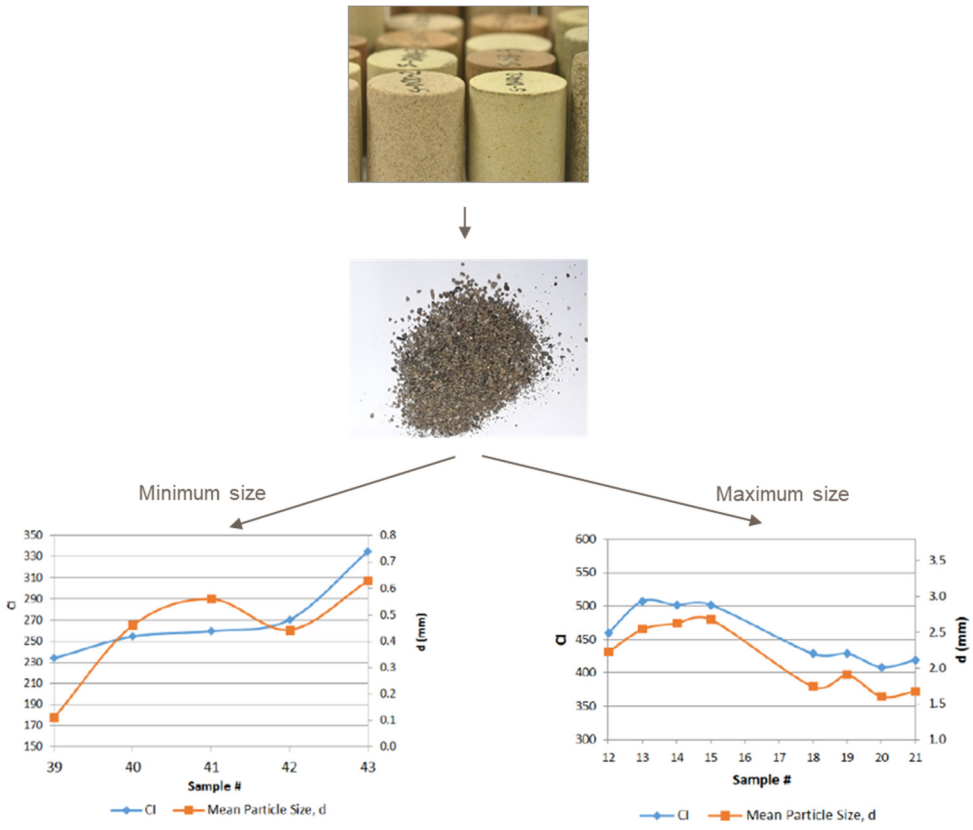


**Figure 3.** Process evaluation of pseudo-cuttings generation from plugs. The particle size distribution plots represent the minimum and maximum obtained sizes based on the coarseness index (CI) and mean particle size (d), defined for several cutting samples ("Sample #") produced during drilling [26].

### *2.4. Thin Section Preparation*

Thin sections were prepared from the end-trims of sandstone plugs. To ensure parallelism of the sample faces, the plugs were carefully ground. Subsequently, the rock samples were impregnated with blue-dyed epoxy resin and meticulously prepared for petrographic thin sections with a final high-quality polishing of metallographic grade.

### *2.5. Thin Section Scan*

Automatic high-resolution scans of the thin sections were conducted using a Zeiss Axio Scan.Z1 whole slide image scanner (Oberkochen, Germany), employing plane polarized light illumination (PPL) at a 10× magnification. The resulting scanned images of the entire thin sections were gigapixel images, comprising multi-resolution image pyramids, with a maximum resolution of 0.44 microns per pixel. Each thin section scan was completed in less than 10 min.

### *2.6. Digital Rock Physics Workflow*

A digital rock physics workflow was developed to compute properties utilizing the high-resolution thin section scans.

The implemented Python code takes 2D PPL images from an automatic thin section scanner as input, allowing for the differentiation between the solid and void phases. The subroutine outputs a range of laboratory properties, including porosity and permeability. The acquisition of these properties involves two main phases: binarization, which distinguishes the pore space from the solid phase, and quantification and characterization of the pore space.

The first step in the processing involves the binarization of the sample. In the PPL images, an unsupervised classification is utilized to segment the resin from the rock or rock fragments. Additionally, an effort has been made to determine the area on which the analysis should be performed in a deterministic and automatic manner. This is necessary because the rock sample captured in the thin sections is often irregular, fragmented, and not always centered in the middle of the glass.

The binarization of cuttings in the thin section follows the same unsupervised technique. Cutting detection and isolation are accomplished by applying a modified version of the marker-based watershed algorithm. An apollonic fill is applied to determine the locations of cutting centroids, assuming that they correspond to the centers of the largest circumferences that can be fitted inside each cutting. These centroids are subsequently used for the marker-based watershed segmentation.

Once the pore space is labeled in the images, a physics-driven approach is adopted to measure all the reservoir properties by characterizing and quantifying the pore space. The calculation of porosity is a straightforward process that involves counting the proportion of pixels labeled as pore and comparing that to the number of pixels labeled as grains to obtain a percentage.

However, the calculation of permeability is more complex. It relies on extracting the pore size distribution using the apollonic algorithm, which fills the pore space with circles representing the actual pore size distribution. Once this distribution is obtained, the calculation of permeabilities can be performed. In this study, Winland's permeability equation [27] was considered. Winland's equation is a simple permeability model suitable for homogeneous and relatively uniform pore size distributions, such as those found in sandstones. It was observed to provide the best fit for scenarios where both laboratory and digital data were obtained.

The size and location of the area to be analyzed are determined using the concept of the representative elementary area (REA). Small areas exhibit significant variations in the measured property, and at a certain size known as the "lambda correlation", the size of the image does not need to be larger, as the property measurement will consistently yield the same value, capturing the heterogeneity of the rock. The developed code measures multiple points (i.e., 5 points/areas) per sample and per image. It is important to note

that the area size representative for one property, such as porosity, also applies to other properties such as permeability.

Cuttings observed in thin sections are classified into different categories based on their optical properties. For each cutting, the mean values of the red, green, and blue channels in the RGB color space, along with the hue, saturation, and value in the HSV color space, are extracted. This vector of information is subsequently used for unsupervised classification using the K-means algorithm. The optimal number of cutting clusters is determined using the Bayesian information criterion (BIC) coefficient, which is calculated for all possible solutions (i.e., different numbers of clusters from 2 to 10) using the aforementioned vector of optical information. Once the cuttings are labeled with their corresponding cluster, it becomes possible to link each label to a specific lithological category.

### *2.7. PETMiner Software*

PETMiner [28] version 3.2.2.3 is a data visualization and mining software designed to enhance the integration of microstructural and petrophysical data. In this study, PETMiner was utilized to establish links between measured and computed petrophysical properties and the corresponding image data. This allowed for the replacement of points on plots with the images where the properties were computed.

### *2.8. Cuttings from Oil and Gas Wells*

The developed DRP workflow was applied to real cuttings obtained from various oil and gas wells operated by Repsol. A total of 223 cutting samples were examined (see Supplementary Materials Table S4). The cuttings were washed and dried on the well rig following standard procedures after drilling. Specific details regarding the well locations and assets have been omitted to ensure confidentiality.

## 3. Results

### *3.1. RCAL Plugs*

The porosity and permeability results obtained from the plug samples (Table 2) demonstrate a range of values, including relatively low porosity (<0.17 porosity fraction) and low permeability (<10 mD), medium porosity (<0.3 porosity fraction) and permeability (<100 mD), as well as high porosity (>0.3 porosity fraction) and permeability (>100 mD). It is also observed that, for each plug sample, there is minimal variability in porosity and permeability, and the reproducibility of measurements using RCAL was consistently excellent after conducting five measurements on each plug (Figure 4), with the exception of sample SS-120 (Salt Wash North).

**Table 2.** Average results from routine core analysis (RCAL) for plug samples.

| ID | Sample ID | Name | Porosity (frac.) | Permeability (mD) |
|---|---|---|---|---|
| 1 | SS-123 | Torrey Buff | 0.17 | 3.2 |
| 2 | SS-100 | Bandera Brown | 0.26 | 84 |
| 3 | SS-109 | Carbon Tan | 0.17 | 53 |
| 4 | SS-121 | San Saba | 0.21 | 68 |
| 5 | SS-106 | Berea Spider | 0.21 | 256 |
| 6 | SS-120 | Salt Wash North | 0.22 | 622 |
| 7 | SS-110 | Castlegate | 0.28 | 801 |

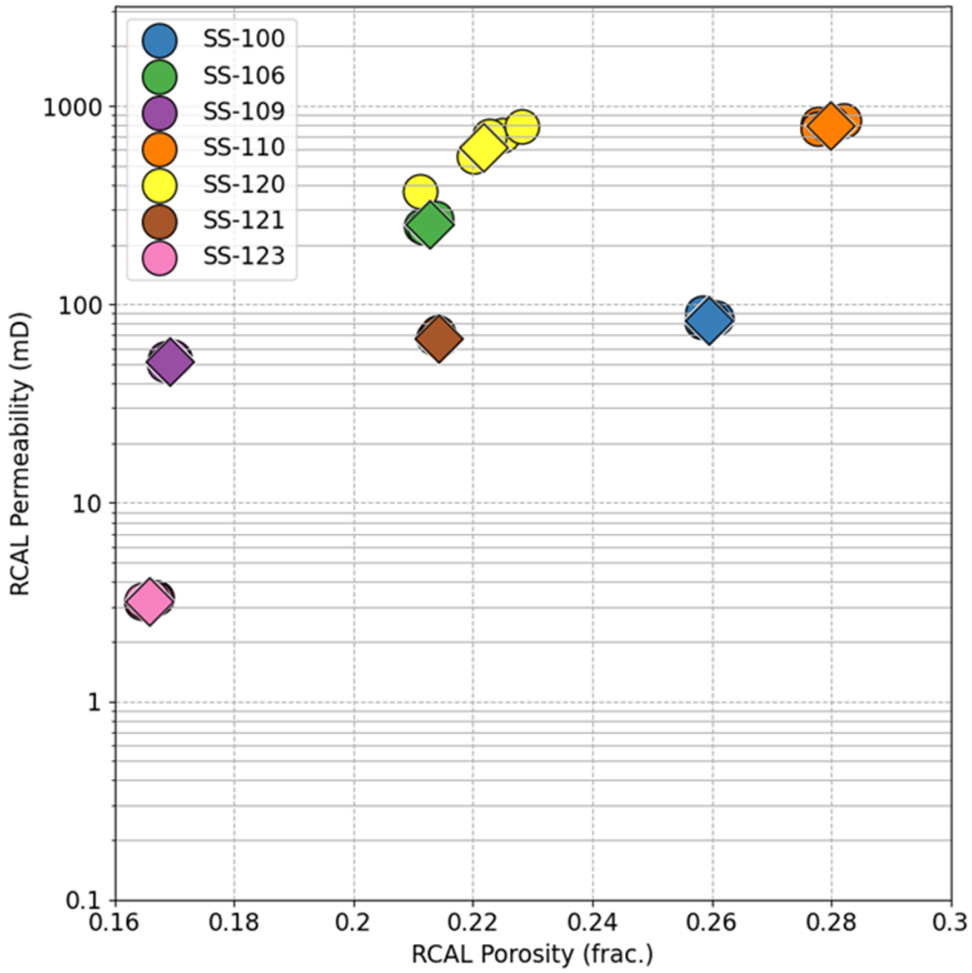


**Figure 4.** Porosity and permeability results from RCAL analysis on plug samples. Average values are represented by diamond symbols.

### *3.2. DRP Plugs*

The porosity and permeability results obtained using the DRP workflow on plug samples are presented in Table 3. These results exhibit the three main groups with relatively low, medium, and high values. Each sample demonstrates some variability in porosity and permeability compared to the average values (Figure 5). For each thin section, multiple porosity and permeability values were computed, corresponding to various measurement areas as outlined in the DRP workflow (i.e., multipoint approach; see Supplementary Materials Table S2).

**Table 3.** Average results from digital rock physics (DRP) analysis for plug samples.

| ID | Sample ID | Name | Porosity (frac.) | Permeability (mD) |
|---|---|---|---|---|
| 1 | SS-123 | Torrey Buff | 0.16 | 2.3 |
| 2 | SS-100 | Bandera Brown | 0.22 | 34 |
| 3 | SS-109 | Carbon Tan | 0.19 | 93 |
| 4 | SS-121 | San Saba | 0.23 | 44 |
| 5 | SS-106 | Berea Spider | 0.25 | 528 |
| 6 | SS-120 | Salt Wash North | 0.23 | 555 |
| 7 | SS-110 | Castlegate | 0.23 | 435 |

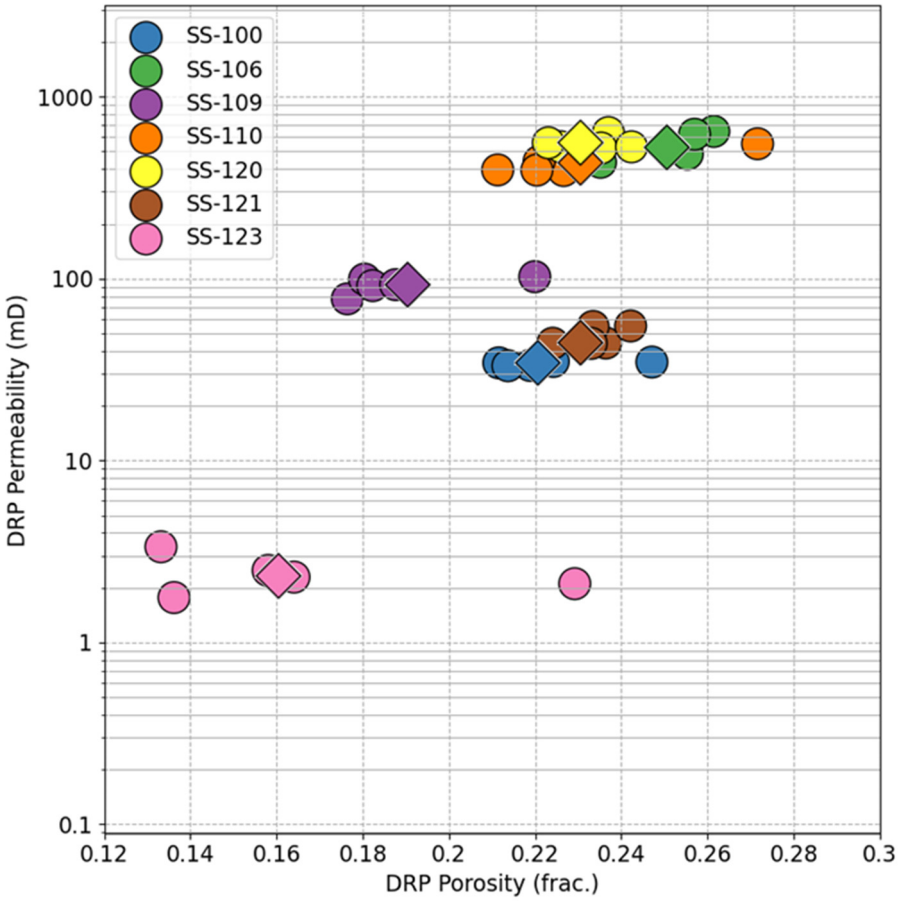


**Figure 5.** Porosity and permeability results from DRP analysis on plug samples. Average values are represented by diamond symbols.

### *3.3. DRP Pseudo-Cuttings*

Hundreds of cuttings were identified and extracted from each thin section for the application of the DRP workflow in order to obtain porosity and permeability properties (Figures 6 and 7).

Porosity and permeability results obtained from the application of the DRP workflow on pseudo-cutting samples are presented in Table 4. These results exhibit a continuous trend of values ranging from relatively low to relatively high (Figure 8). A total of over 800 porosity and permeability points were obtained for the seven studied sandstone samples, with more than 100 measured points per sample (see Supplementary Materials Table S3).

**Table 4.** Average results from digital rock physics (DRP) analysis for pseudo-cutting samples.

| ID | Sample ID | Name | Porosity (frac.) | Permeability (mD) |
|---|---|---|---|---|
| 1 | SS-123 | Torrey Buff | 0.16 | 3.4 |
| 2 | SS-100 | Bandera Brown | 0.19 | 26 |
| 3 | SS-109 | Carbon Tan | 0.19 | 55 |
| 4 | SS-121 | San Saba | 0.2 | 40 |
| 5 | SS-106 | Berea Spider | 0.25 | 172 |
| 6 | SS-120 | Salt Wash North | 0.22 | 158 |
| 7 | SS-110 | Castlegate | 0.25 | 220 |

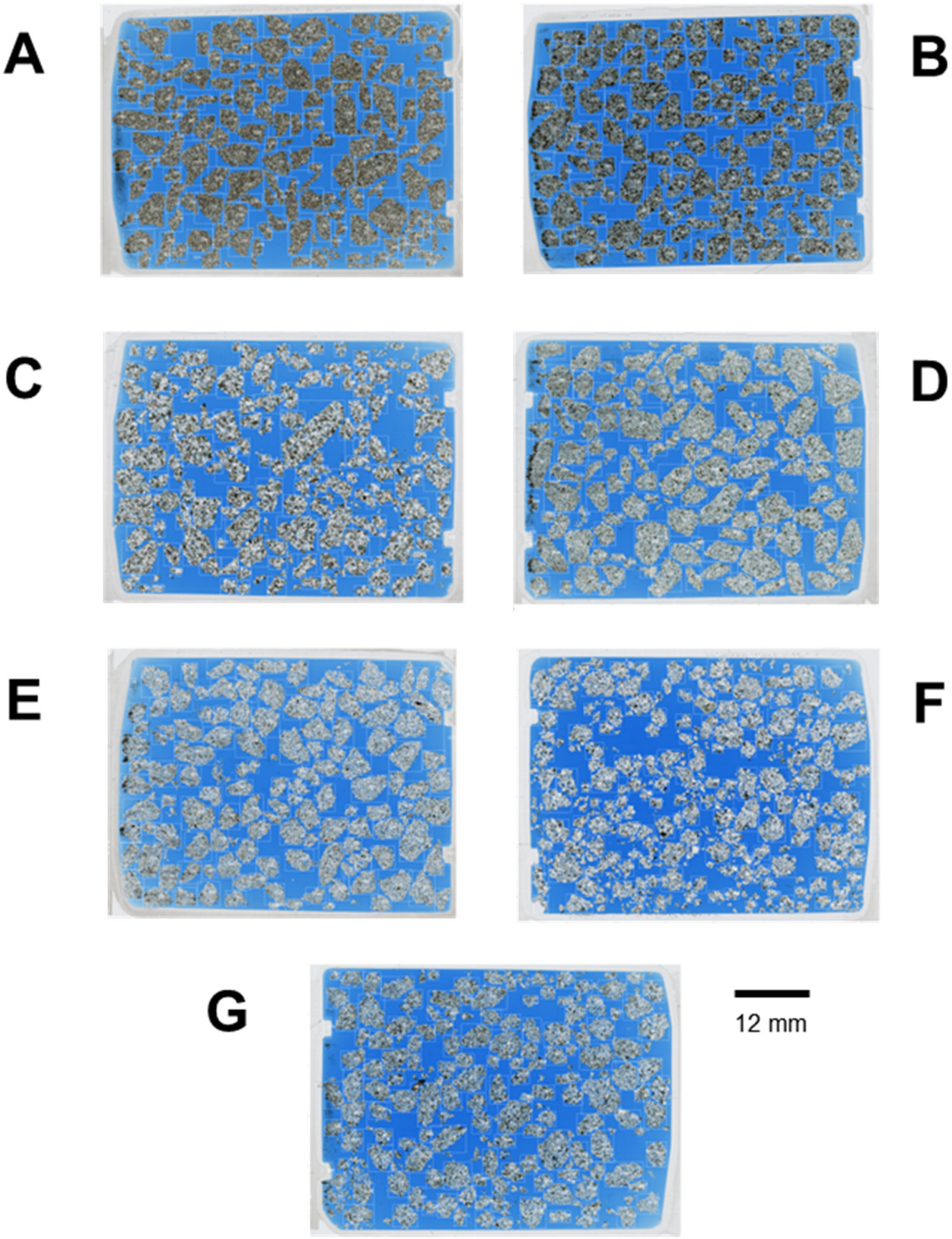


**Figure 6.** High-resolution thin section scan images displaying the bounding boxes of identified cuttings that were cropped and processed using the DRP workflow. Torrey Buff (**A**), Bandera Brown (**B**), Carbon Tan (**C**), San Saba (**D**), Berea Spider (**E**), Salt Wash North (**F**), and Castlegate (**G**).

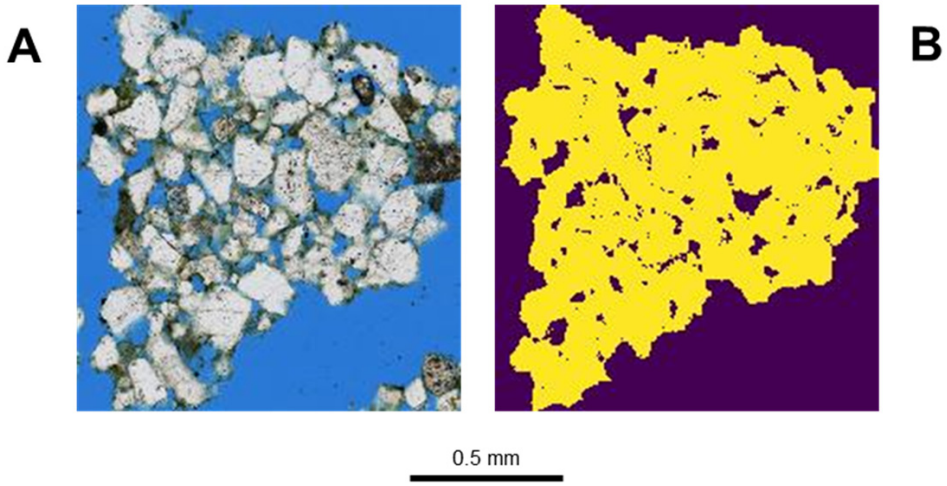


**Figure 7.** An example of one of the bounding boxes (**A**) demonstrating the outcome of the segmentation process (**B**).

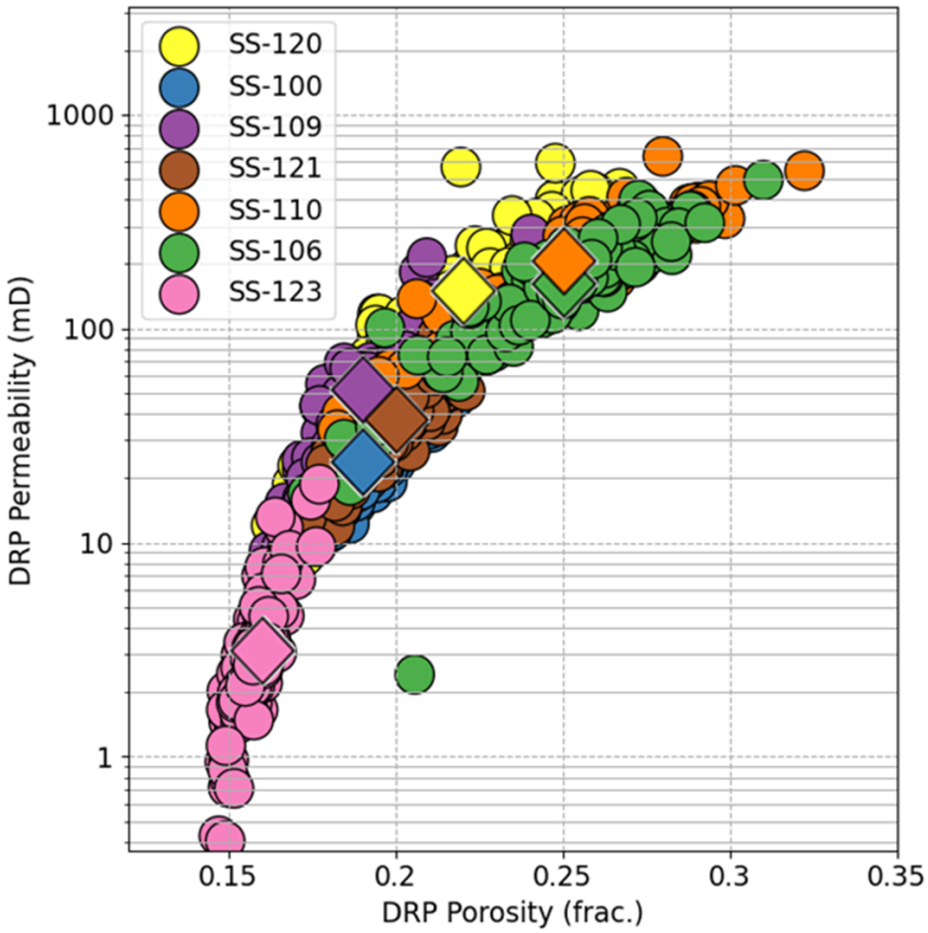


**Figure 8.** Porosity and permeability results from DRP analysis on pseudo-cuttings. Average values are represented by diamond symbols.

### *3.4. DRP Cuttings from Oil and Gas Wells*

Tens to hundreds of cuttings were identified and extracted from each thin section of real cuttings obtained from the five tight sandstone oil and gas wells (Figure 9).

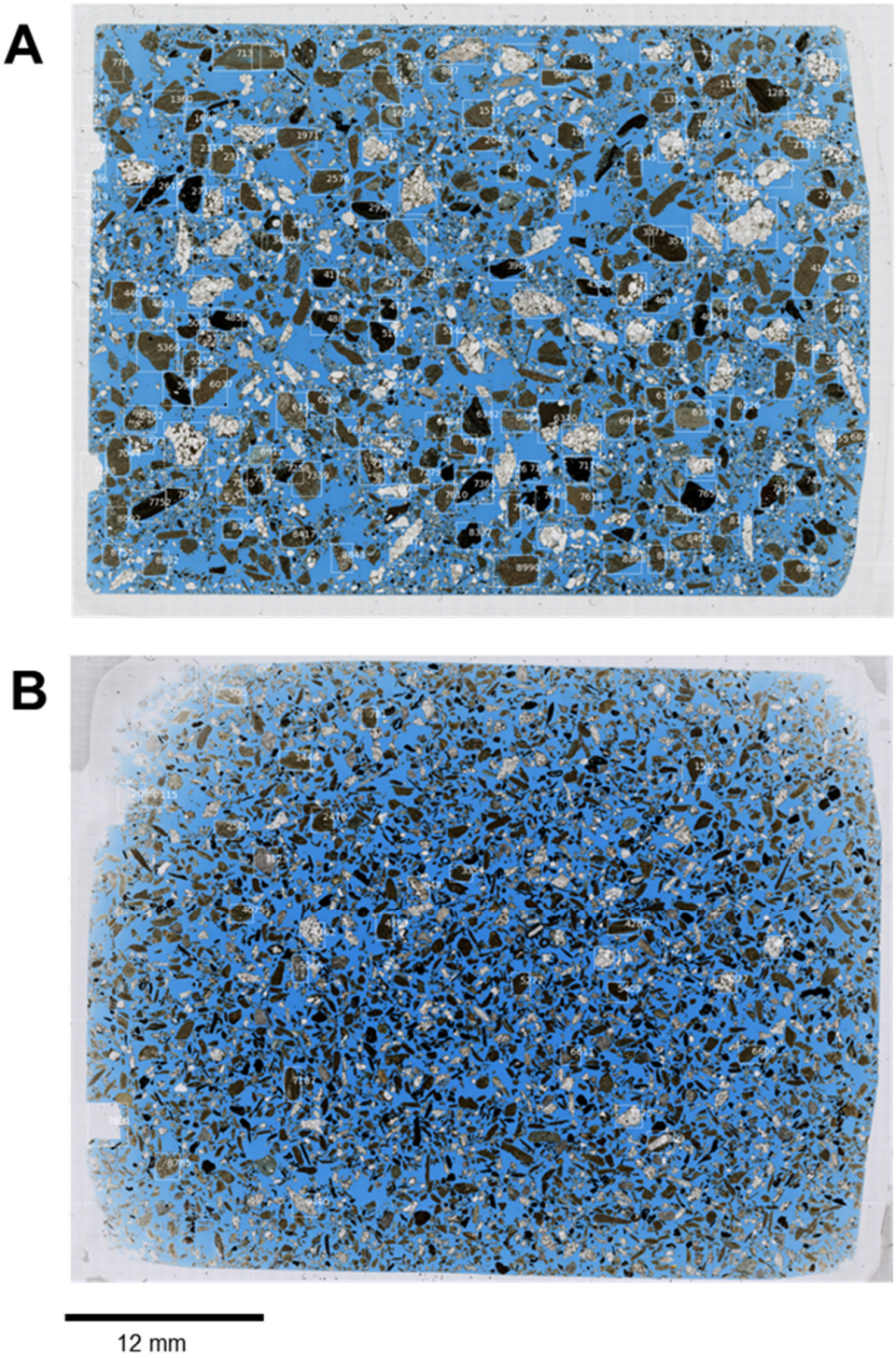


**Figure 9.** High-resolution thin section scan images showcasing examples of the bounding boxes of identified cuttings that were cropped and processed using the DRP workflow from a selection of the five Repsol oil and gas wells studied. Note the variation in cutting sizes between the samples (**A**,**B**) from a real oil and gas well, as no sieving was performed before thin section preparation.

Porosity and permeability properties were obtained using the DRP workflow on the real cuttings (Figure 10), revealing a continuous trend of porosity and permeability values from low to relatively high.

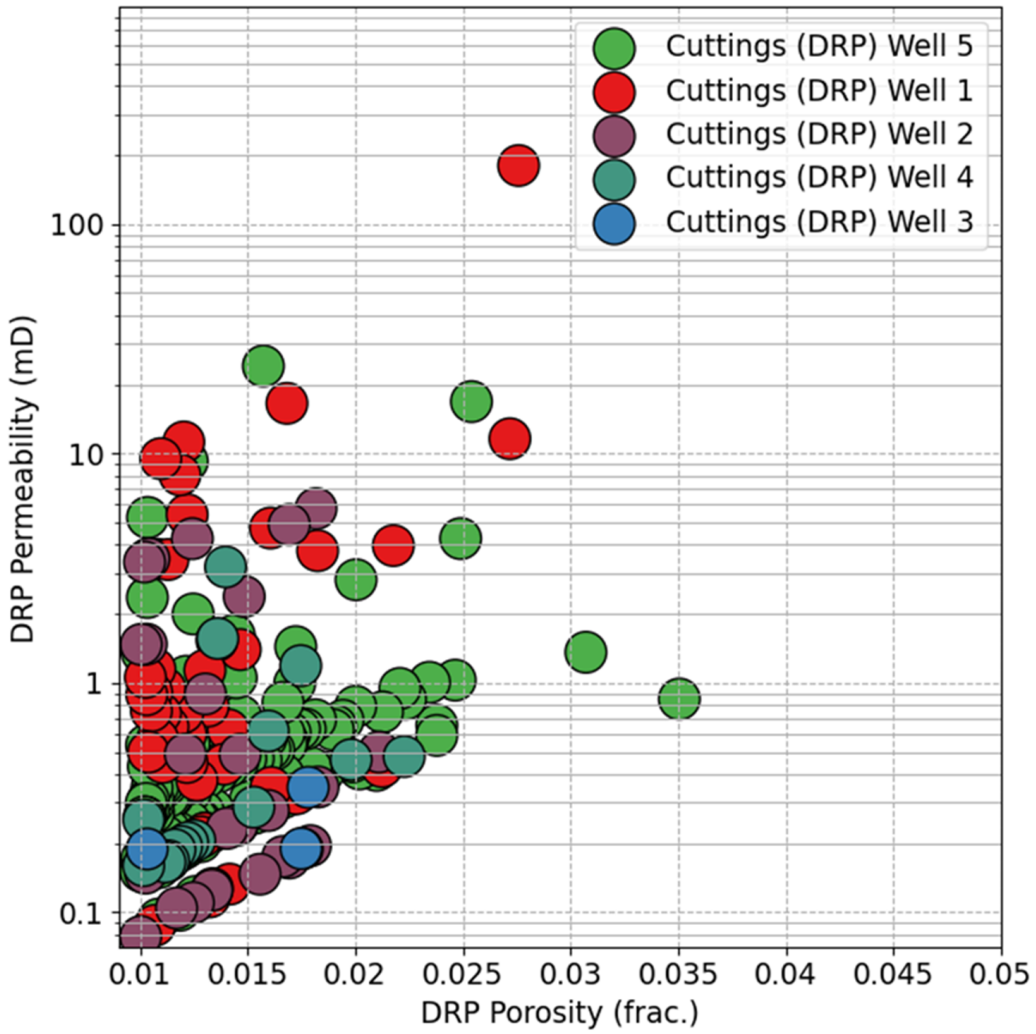


**Figure 10.** Porosity and permeability results from DRP analysis on real cuttings from five oil and gas wells.

## 4. Discussion

### *4.1. RCAL vs. DRP in Plugs and Pseudo-Cuttings*

A comparison of the average values from DRP and RCAL (Figure 11) in plugs and pseudo-cuttings indicates that DRP provides comparable porosity and permeability values, falling below one standard deviation, for the low, medium, and high permeability groups of samples, with the exception of sample SS-100 (Bandera Brown). The implementation of the DRP workflow enables an understanding of why certain samples exhibit a wide range of variability in porosity and permeability properties when using the DRP approach (Figure 12). This variability appears to be associated with non-homogeneous textures characterized by moderate clay content and iron-rich grains, which could potentially influence the values obtained through the DRP analysis in different cropped areas.

The comparison of DRP porosity and permeability results from pseudo-cuttings and average RCAL results from plugs (Figure 13), as well as average DRP results from plug samples (Figure 14), reveals that the average values obtained from RCAL and DRP on plugs align with the continuous trend of porosity and permeability values observed in the pseudo-cuttings.

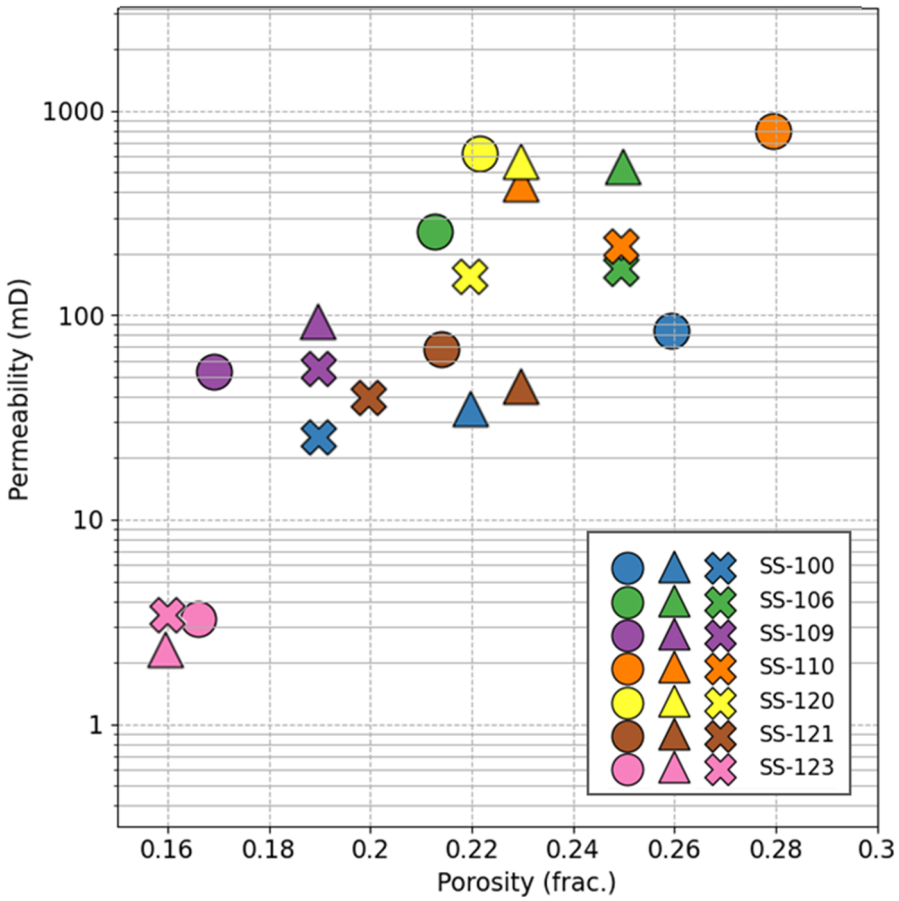


**Figure 11.** Plot of average porosity and permeability values for RCAL plug samples (circles), DRP plugs (triangles), and DRP pseudo-cuttings (crosses).

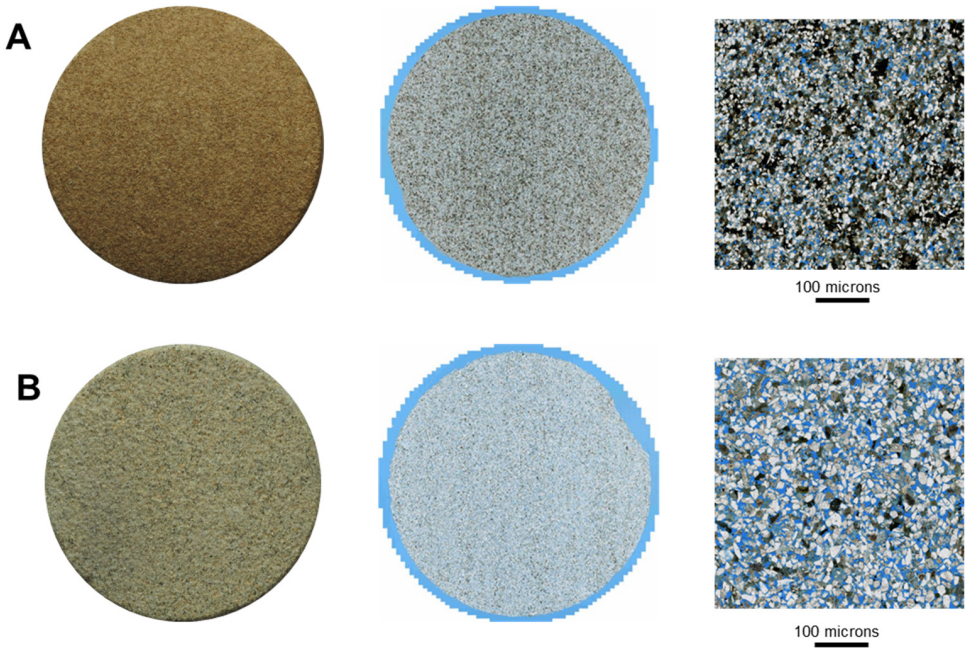


**Figure 12.** Comparison of plug photography (**left**), high-resolution thin section scan of plugs (**center**), and cropped area photomicrograph for the DRP workflow (**right**). It is observed that sample SS-100 Bandera Brown (**A**) exhibits non-homogeneous composition and texture, in contrast to sample SS-110 Castlegate (**B**). Plug samples have a diameter of 1.5 inches.

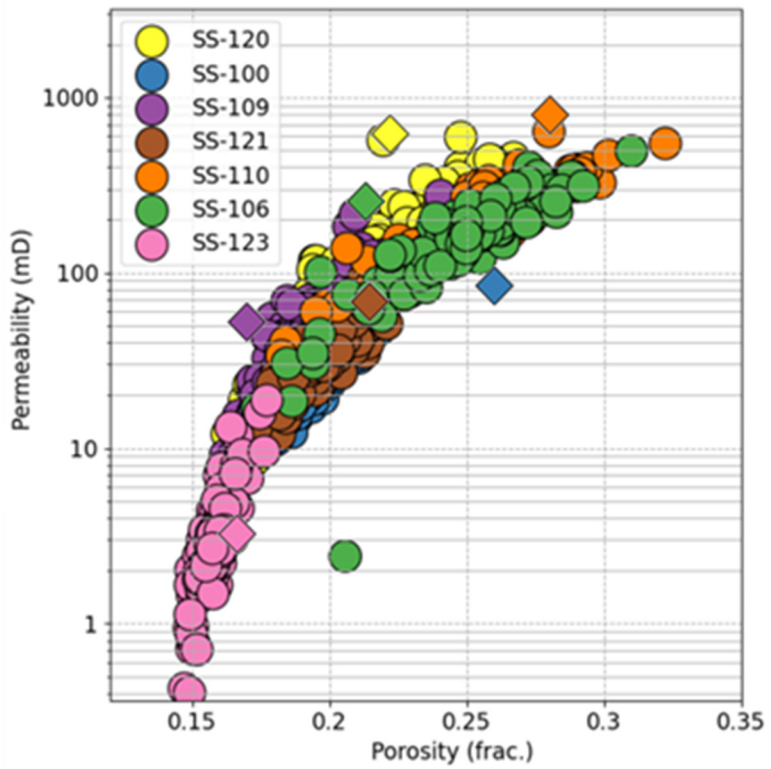


**Figure 13.** Comparison of average porosity and permeability values from DRP pseudo-cuttings and RCAL plugs (diamond symbols).

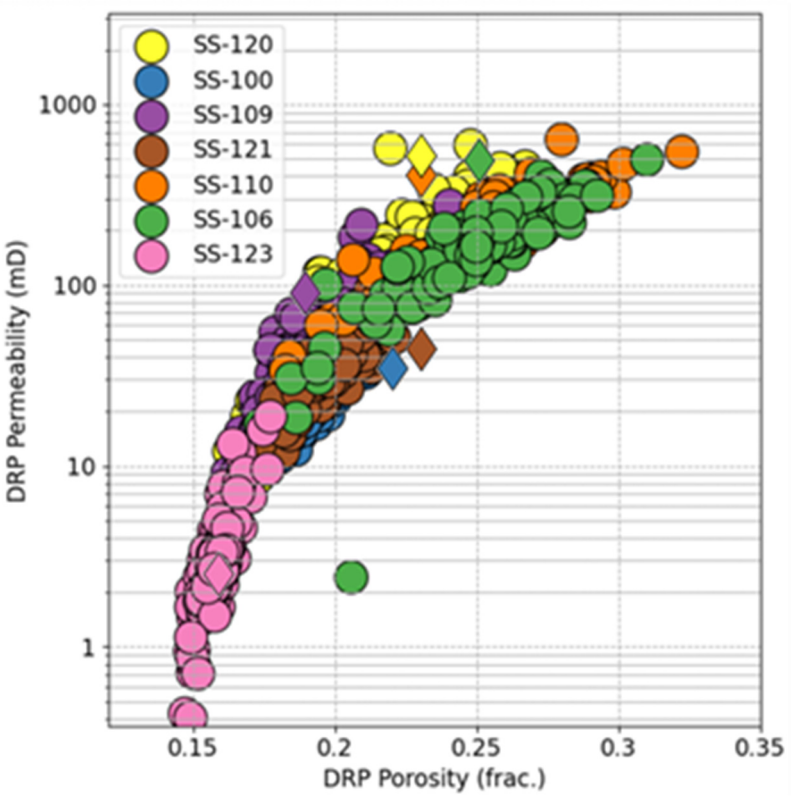


**Figure 14.** Comparison of average porosity and permeability values from DRP pseudo-cuttings and DRP plugs (diamond symbols).

It is important to highlight that the RCAL values correspond to a 3D volume of the rock, and the obtained results represent an average across the entire rock volume. On the other hand, the DRP approach allows for the computation of more points, but only within the area of the plug where the thin section was prepared. This can lead to more variability in the average porosity and permeability values when compared to RCAL (Figure 15).

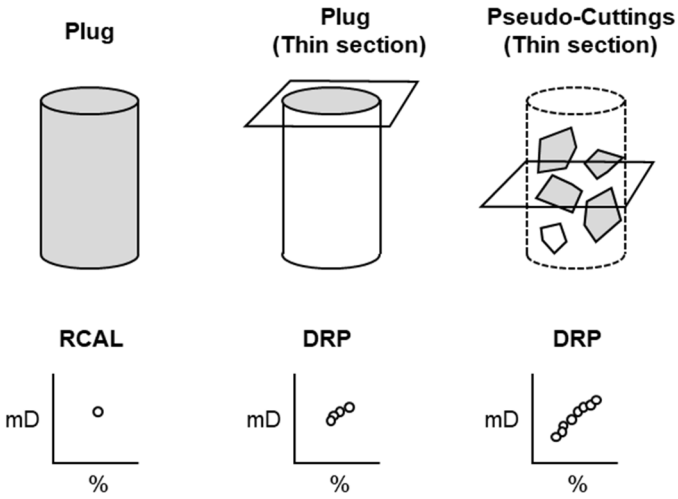


**Figure 15.** Illustration depicting the comparison between different sample types (plug, thin section, and pseudo-cuttings) and the measurement/computation of porosity and permeability using RCAL and DRP. The shaded area represents the region or volume where the property (conceptually) is measured or computed.

### *4.2. DRP in Real Cuttings*

As the real cutting samples correspond to tight sandstone reservoirs, the obtained porosity and property values are relatively low but consistent with the expected values for such reservoirs.

It is important to mention that the size of the cuttings varied in the real cutting samples, as no sieving was performed before thin section preparation to avoid time-consuming sample manipulation and potential biases. The relatively small size of the cuttings in some samples hindered their identification and extraction for processing (Figure 9). Moreover, these small-sized cuttings likely do not meet the minimum representative elementary area (REA) required for computation to obtain petrophysical properties.

One limitation of applying a DRP workflow to extract petrophysical properties from cuttings is the use of polycrystalline-diamond compact (PDC) bits during drilling. These bits have the potential to pulverize all or parts of the rock fabric, resulting in bit flour, clay, or sand [29,30]. As a result, the rock texture can be altered by PDC bits, generating platelets and other artifacts that range from minor textural alterations to extensive drill-bit metamorphism (DBM). In cases of DBM, partial melting and quenching can even lead to the formation of glassy cuttings [31]. Consequently, the loss of the original rock texture or alteration of the cuttings hinders the application of a DRP workflow.

### *4.3. DRP Workflow and Image Data*

One of the advantages of the DRP workflow is the ability to link the computed petrophysical properties with image data, allowing for the replacement of points on plots with the corresponding images where the properties were computed. The image data can encompass various types of images acquired from the rock sample. In this study, high-resolution thin section images, cropped areas, and segmented areas were used (Figures 16–19).

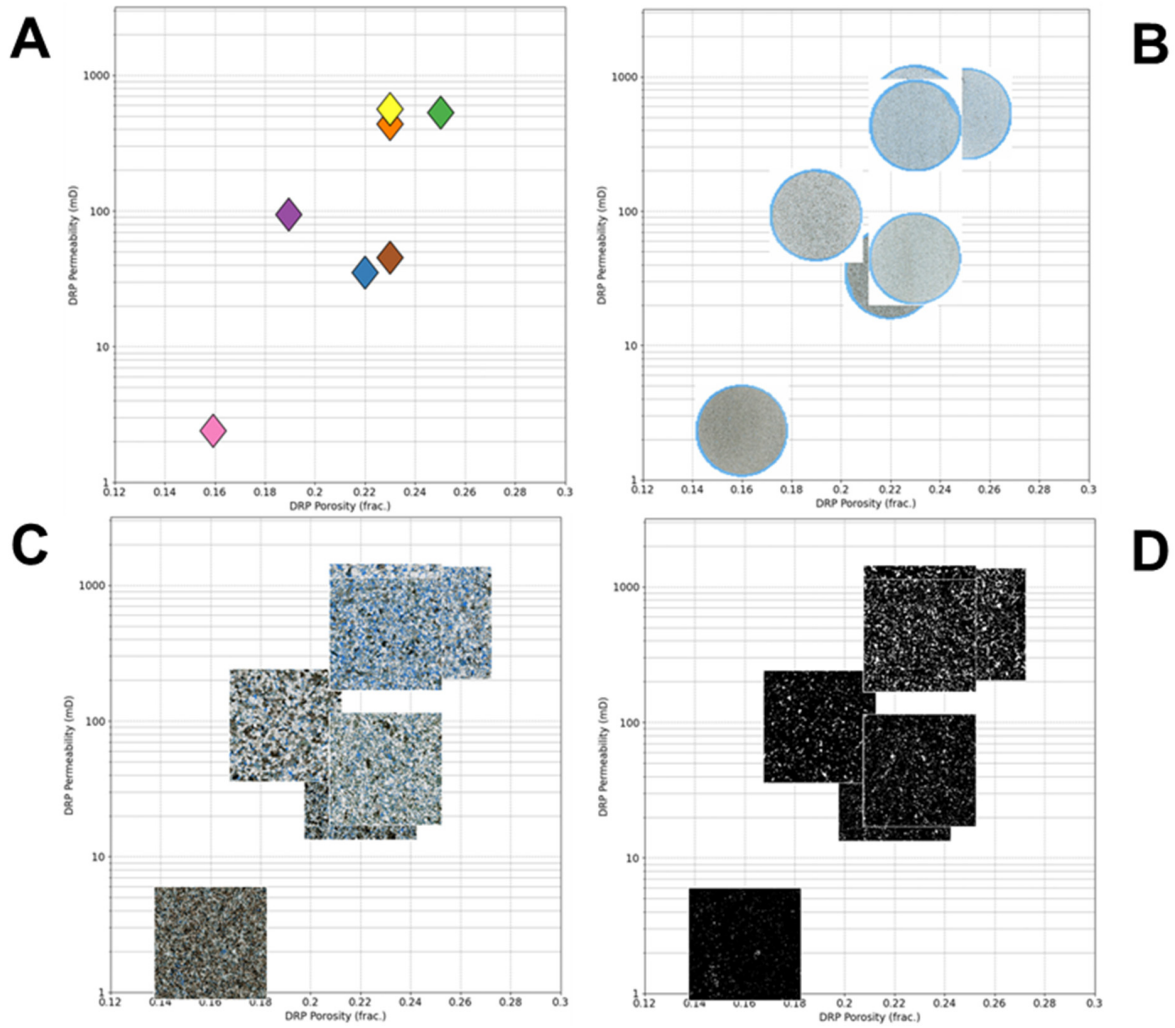


**Figure 16.** Example of average porosity and permeability values obtained by DRP in plugs (**A**), high-resolution thin section scan images ((**B**); 1.5 inches in diameter), cropped areas (**C**), and segmented areas ((**D**); 500 × 500 microns).

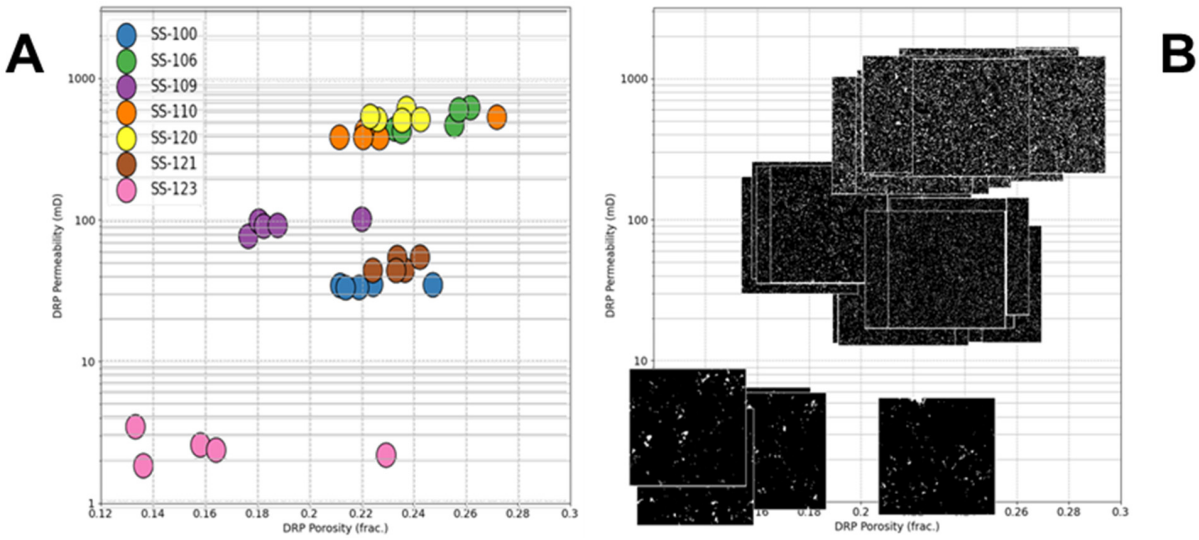


**Figure 17.** Porosity and permeability values obtained by DRP in plugs using the multipoint approach (**A**) and segmented areas (**B**).

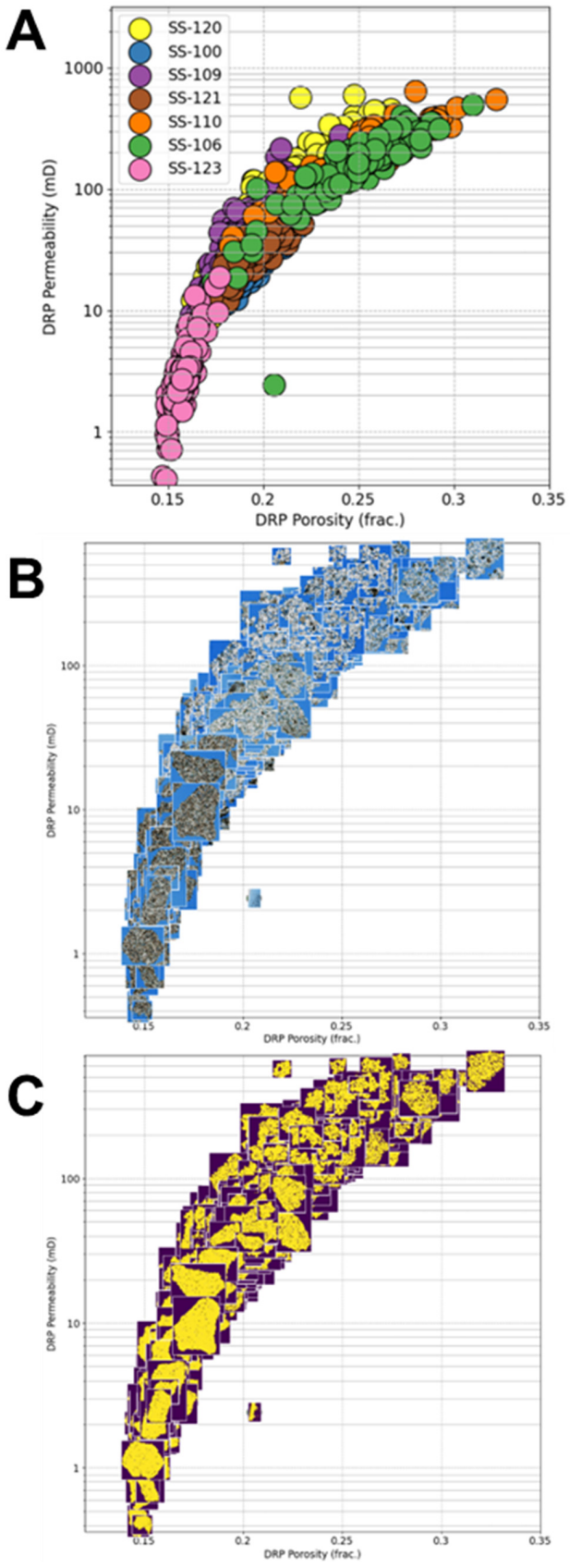


**Figure 18.** Example of porosity and permeability properties (**A**) computed using the developed DRP workflow in pseudo-cuttings. (**B**) correspond to cropped (**B**), and segmented (**C**) images where properties where obtained.

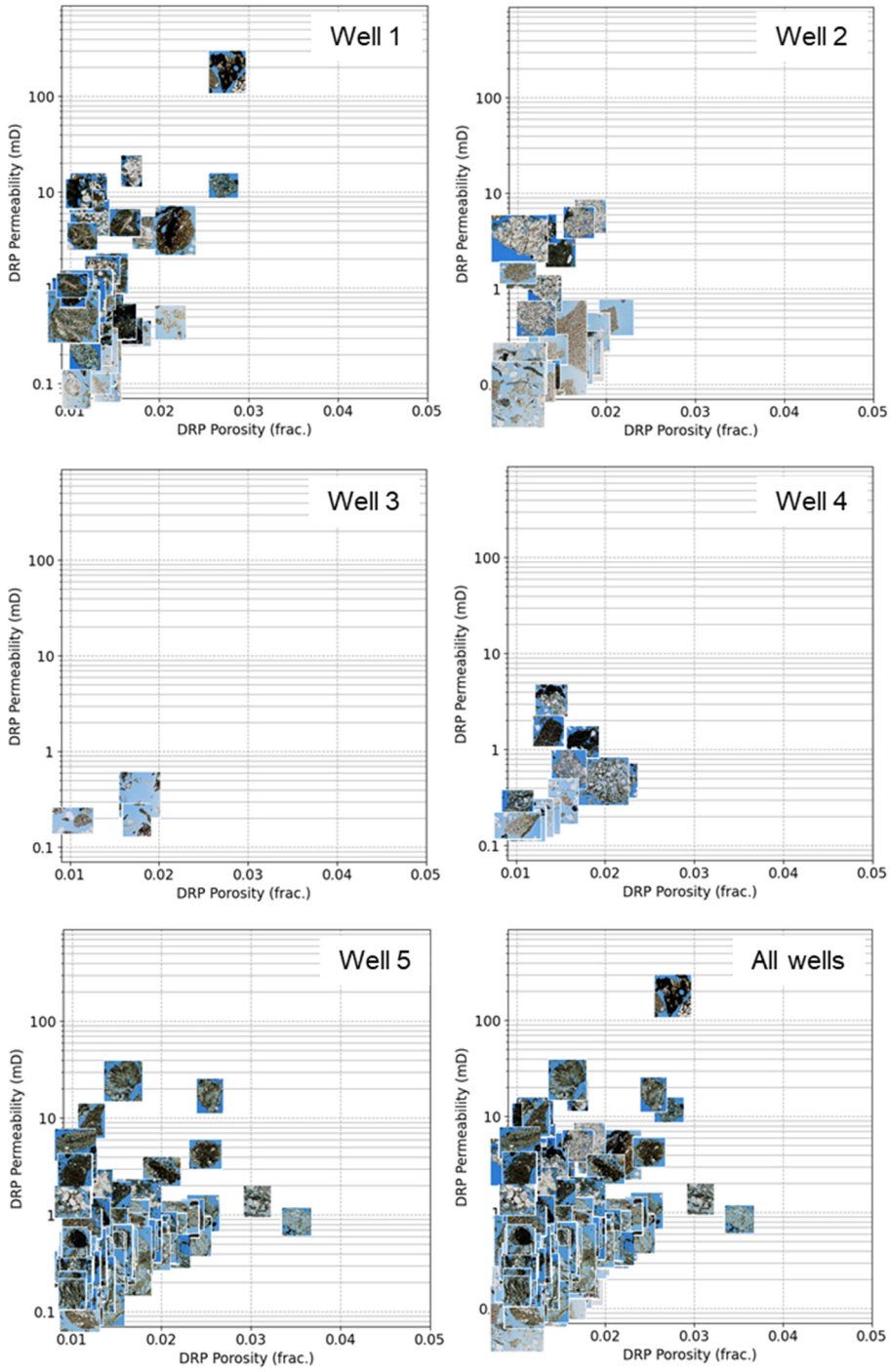


**Figure 19.** Cropped areas after identifying bounding box cuttings to compute porosity and permeability following the DRP workflow in real cuttings from five wells. From left to right: Well 1 to Well 5. The bottom right plot corresponds to cuttings from all wells.

The use of clustering analyses in real cutting samples, combined with the ability to observe the plane polarized light (PPL) image corresponding to each cutting within a defined cluster, facilitated the identification and assignment of a lithology to each clustering class (Figure 20). Additionally, this approach could aid in the identification of artifacts, exotic materials, or loss circulation material typically found in the cutting samples.

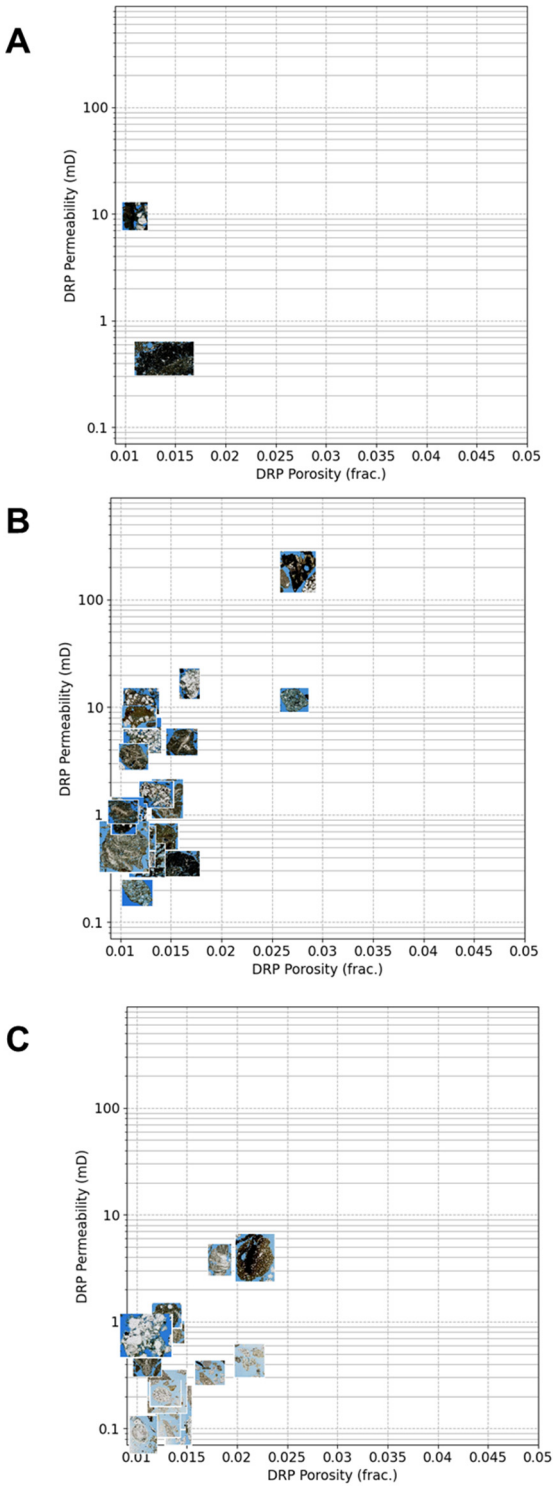


**Figure 20.** Example of three clusters defined in one well: Cluster 1 (**A**) corresponds to claystones, Cluster 2 (**B**) corresponds to fine-grained sandstones, and Cluster 3 (**C**) corresponds to coarse-grained sandstones.

### *4.4. DRP Time, Cost, and Added Value*

The described and applied DRP workflow provides porosity and permeability results within minutes for each sample using a modest and cost-effective virtual machine. When comparing DRP with RCAL, it is not necessary to argue that the cost and time required for analyzing porosity and permeability in the laboratory are also low-cost and fast. However,

it is crucial to note that RCAL analysis requires a perfectly cylindrical plug sample. In cases where plug samples are damaged, unconsolidated, or unavailable, or in any other situation that prevents the measurement of petrophysical properties in the lab, the DRP workflow offers flexibility by allowing the acquisition of petrophysical properties using various sample types, including cuttings. In essence, the DRP approach enables the use of any kind of rock material.

Furthermore, the utilization of high-resolution thin section images obtained from automatic thin section scanners has contributed to reducing computation time, as the generated files are relatively small compared to other image acquisition techniques.

In terms of cost, each analysis conducted through the DRP workflow is relatively inexpensive. It requires the production of a thin section, a high-resolution thin section scan, and the execution of the DRP code on a modest virtual machine with a significantly reduced price per hour.

It is important to note that plug samples are not always readily available for RCAL analysis, yet the need for petrophysical properties remains crucial in reducing subsurface uncertainty and improving geological modeling. In other instances, although plug samples may be available, they may not possess the ideal shape, such as perfect cylindrical form, or their preservation status may be compromised, possibly due to previous SCAL analysis or being part of legacy samples. Furthermore, plug samples may not always be accessible, as they are often guarded by operators or national oil companies who hold ownership rights over subsurface rock materials.

## 5. Conclusions

The development of the DRP workflow was showcased, beginning with the utilization of homogeneous reference plug samples obtained from sandstone quarries to obtain RCAL properties. Subsequently, the DRP workflow was applied to compute porosity and permeability properties, allowing for a comparison with RCAL results. The workflow was further enhanced by generating pseudo-cuttings from plugs, enabling a more comprehensive analysis of cuttings. The results obtained from comparing RCAL, plugs DRP, and pseudo-cuttings DRP demonstrated the statistical equivalence of porosity and permeability values to those obtained from plug rock samples. Moreover, the application of the DRP workflow to real oil and gas reservoir cuttings successfully identified the presence of different lithologies without interfering with the computation of petrophysical properties.

In summary, this study emphasizes the importance and value of the DRP workflow as a relatively fast and cost-effective procedure for extracting petrophysical properties, specifically porosity and permeability. It proves to be especially useful when only cutting samples are available, or when plug rock samples are unsuitable or unavailable for laboratory analysis. The DRP workflow utilizes high-resolution thin section scan images, providing the added advantage of obtaining more comprehensive data from the samples through a multipoint approach and the ability to link computed petrophysical properties to the corresponding image data from the rock plugs and cuttings.

Finally, the added value of implementing the DRP workflow in oil and gas reservoir characterization, specifically with plug and cutting samples using thin sections, holds significance in the current global energy transition context. This includes activities such as carbon capture, carbon sequestration, and geothermal operations, where core or plug samples may not be obtained, but cuttings are always available. By leveraging the DRP workflow, valuable insights can be gained, contributing to enhanced reservoir understanding and decision-making in these evolving energy sectors.

**Supplementary Materials:** The following supporting information can be downloaded at: https://www.mdpi.com/article/10.3390/min13091140/s1, Table S1: Routine Core Analysis (RCAL) results for plugs samples; Table S2: Digital Rock Physics (DRP) results for plugs samples; Table S3: Digital Rock Physics (DRP) results for pseudo-cuttings samples; Table S4: Digital Rock Physics (DRP) results for cuttings samples.

**Author Contributions:** Envisioning, conceptualization, project administration M.Á.C. and C.A.S.; methodology, C.A.S. and J.N.C.; laboratory experiments V.B.; digital image acquisition J.L.P.-J. and P.R.F.-D.; algorithms development and validation, J.N.C., J.L.P.-J., P.R.F.-D., S.E. and J.R.C.; writing—original draft preparation, M.Á.C.; writing—review and editing, T.B.-A. and J.D.M.-M. All authors have read and agreed to the published version of the manuscript.

**Funding:** This research was supported by Repsol Technology Lab.

**Data Availability Statement:** The complete data set obtained during this research is shared in the Supplementary Materials section.

**Conflicts of Interest:** The authors declare no conflict of interest. The funders had no role in the design of the study; in the collection, analyses, or interpretation of data; in the writing of the manuscript; or in the decision to publish the results.

## References

1. Dvorkin, J.; Armbruster, M.; Baldwin, Q.; Derzhi, N.; Gomez, C.; Nur, B.; Nur, A.; Mu, Y. The future of rock physics: Computational methods vs. lab testing. *First Break.* **2008**, *26*, 63–68. [CrossRef]
2. Balcewicz, M.; Siegert, M.; Gurris, M.; Ruf, M.; Krach, D.; Steeb, H.; Saenger, E.H. Digital Rock Physics: A Geological Driven Workflow for the Segmentation of Anisotropic Ruhr Sandstone. *Front. Earth Sci.* **2021**, *9*, 19. [CrossRef]
3. Riepe, L.; Knackstedt, M. Quantitative Mineralogical and Petrophysical Analysis of Cuttings. In Proceedings of the Petroleum Geoscience Conference & Exhibition, Kuala Lumpur, Malaysia, 18–19 March 2013; European Association of Geoscientists & Engineers: Utrecht, The Netherlands, 2013; p. 4.
4. Andrä, H.; Combaret, N.; Dvorkin, J.; Glatt, E.; Han, J.; Kabel, M.; Keehm, Y.; Krzikalla, F.; Lee, M.; Madonna, C.; et al. Digital rock physics benchmarks—Part I: Imaging and segmentation. *Comput. Geosci.* **2013**, *50*, 25–32. [CrossRef]
5. Jouini, M.S.; Keskes, N. Numerical estimation of rock properties and textural facies classification of core samples using X-ray Computed Tomography images. *Appl. Math. Model.* **2017**, *41*, 562–581. [CrossRef]
6. Jouini, M.S.; Gomes, J.S.; Tembely, M.; Ibrahim, E.R. Upscaling Strategy to Simulate Permeability in a Carbonate Sample Using Machine Learning and 3D Printing. *IEEE Access* **2021**, *9*, 90631–90641. [CrossRef]
7. Sun, H.; Tao, G.; Vega, S.; Al-Suwaidi, A. Simulation of gas flow in organic-rich mudrocks using digital rock physics. *J. Nat. Gas Sci. Eng.* **2017**, *41*, 17–29. [CrossRef]
8. Verri, I.; Della Torre, A.; Montenegro, G.; Onorati, A.; Duca, S.; Mora, C.A.; Radaelli, F. Development of a Digital Rock Physics workflow for the analysis of sandstones and tight rocks. *J. Nat. Gas Sci. Eng.* **2017**, *156*, 790–800. [CrossRef]
9. Arns, C.H.; Knackstedt, M.A.; Pinczewski, W.V.; Martys, N.S. Virtual permeametry on microtomographic images. *J. Pet. Sci. Eng.* **2004**, *45*, 41–46. [CrossRef]
10. Pérez-Jiménez, J.L.; Caja, M.A.; Peña, A.C.; Blázquez, V.; Santos, C.A.; García-Diego, L.; Sánchez Pérez-Cejuela, V.; Palomares, E.; Bover-Arnal, T.; Martín-Martín, J.D. Digital Rock Physics in Drill Cuttings. In Proceedings of the ResTech2020 Virtual Reservoir Conference, Online, 22 April 2020; European Association of Geoscientists & Engineers: Utrecht, The Netherlands, 2020; p. 2.
11. Menéndez, B.; Christian, D.; Nistal, A. Confocal scanning laser microscopy applied to the study of pore and crack networks in rocks. *Comput. Geosci.* **2001**, *27*, 1101–1109. [CrossRef]
12. Hurley, N.F.; Zhang, T.; Zhao, W.; Xu, G. Confocal Microscopy—A New Way to Model Carbonate Porosity in 3D. In Proceedings of the AAPG GEO 2010 Middle East Geoscience Conference & Exhibition, Manama, Bahrain, 7–10 March 2010; European Association of Geoscientists & Engineers: Utrecht, The Netherlands, 2010; p. 1.
13. Al Ibrahim, M.A.; Hurley, N.F.; Zhao, W.; Acero-Allard, D. An automated PIA system: Capillary pressure curves using confocal microscopy. In Proceedings of the SPE Annual Technical Conference and Exhibition, San Antonio, TX, USA, 8–10 October 2012; OnePetro: Richardson, TX, USA, 2012; SPE-159180-MS, p. 21.
14. Shah, S.M.J.; Yang, J.; Crawshaw, P.; Gharbi, O.; Boek, E.S. Predicting porosity and permeability of carbonate rocks from core-scale to pore-scale using medical CT, confocal laser scanning microscopy and micro CT. In Proceedings of the Society of Petroleum Engineers Annual Technical Conference and Exhibition, New Orleans, LA, USA, 30 September–2 October 2013; SPE: San Antonio, TX, USA, 2013; SPE-166252-MS, p. 13. [CrossRef]
15. Shah, S.M.; Crawshaw, P.; Boek, E.S. Threedimensional imaging of porous media using confocal laser scanning microscopy. *J. Microsc.* **2017**, *265*, 261–271. [CrossRef] [PubMed]
16. Caja, M.A.; Pérez-Jiménez, J.L.; León, M.F.; Acero-Allard, D. Confocal laser scanning microscopy and automated petrographic image analysis in different rock types: Two-dimensional images capillary pressure curves estimation and three-dimensional porosity reconstruction. *AAPG Bull.* **2019**, *103*, 1963–1978. [CrossRef]
17. Caja, M.A.; Santos, C.A.; García, L.; Fernández, P.R.; Pérez, J.L.; Peña, A.; Canal, J.; Blázquez, V.; González, H.; Sánchez, V.; et al. Characterizing Algeria tight reservoir cutting samples with Virtual Microscopy, Petrography, Mineralogy and Digital Petrophysics. In Proceedings of the EAGE/ALNAFT Geoscience Workshop, Algiers, Africa, 28–29 January 2019; European Association of Geoscientists & Engineers: Utrecht, The Netherlands, 2019; p. 5.
18. Crabtree, M. Algorithm Development of a PIA System. Ph.D. Thesis, The University of Tulsa, Tulsa, OK, USA, 1983.

19. Ehrlich, R.; Kennedy, S.K.; Crabtree, S.J.; Cannon, R.L. PIA. Pt 1 analysis of reservoir pore complexes. *J. Sediment. Petrol.* **1984**, *54*, 1365–1378.
20. Korkowitz, J.P. Estimation of petrophysics from thin sections—PIA. *AAPG Bull.* **1987**, *71*, 2.
21. James, H. Application of PIA to the characterization of fluid-flow pathways in a highly-cemented reservoir. *J. Pet. Sci. Eng.* **1995**, *13*, 141–154. [CrossRef]
22. Caja, M.A.; Peña, A.C.; Campos, J.R.; García Diego, L.; Tritlla, J.; Bover-Arnal, T.; Martín-Martín, J.D. Image processing and machine learning applied to lithology identification, classification and quantification of thin section cutting samples. In Proceedings of the SPE Annual Technical Conference and Exhibition, Calgary, AB, Canada, 30 September–2 October 2019; OnePetro: Richardson, TX, USA, 2019; SPE-196117-MS, p. 8.
23. Peña, A.; Caja, M.A.; Campos, J.R.; Santos, C.A.; Pérez, J.L.; Fernández, P.R.; Tritlla, J. Application of Machine Learning models in thin sections image of drill cuttings: Lithology classification and quantification (Algeria tight reservoirs). In Proceedings of the EAGE/ALNAFT Geoscience Workshop, Algiers, Africa, 28–29 January 2019; European Association of Geoscientists & Engineers: Utrecht, The Netherlands, 2019; p. 5.
24. López-García, J.; Caja, M.A.; Peña, A.C.; Nadukandi, P. Automatic lithological classification and quantification in thin-sections of drill cuttings, 2020. In Proceedings of the ResTech2020 Virtual Reservoir Conference, Online, 22 April 2020; European Association of Geoscientists & Engineers: Utrecht, The Netherlands, 2019; p. 2.
25. *ASTM D422-63 2007-e2*; Standard Test Method for Particle-Size Analysis of Soils. ASTM International: West Conshohocken, PA, USA, 2007. Available online: https://www.astm.org/ (accessed on 28 August 2023).
26. Reyes, R.; Kyzym, I.; Rana, P.S.; Molgaard, J.; Butt, S.D. Cuttings Analysis for Rotary Drilling Penetration Mechanisms and Performance Evaluation. In Proceedings of the ARMA US Rock Mechanics/Geomechanics Symposium, San Francisco, CA, USA, 29 June–1 July 2015; OnePetro: Richardson, TX, USA, 2015; ARMA 15-764, p. 9.
27. Winland, H.D. Oil Accumulation in Response to Pore Size Changes. In *Amoco Production Research Report*; Amoco Production Company: Weyburn Field, SK, Canada, 1972; No. F72-G-25.
28. PETMiner Software. Available online: http://www.petriva.co.uk/en/software-new/ (accessed on 28 August 2023).
29. Graves, W. Bit-Generated Rock Textures and Their Effect on Evaluation of Lithology, Porosity, and Shows in Drill-Cutting Samples. *AAPG Bull.* **1986**, *70*, 1129–1135.
30. Wenger, L.M.; Pottorf, R.J.; Macleod, G.; Otten, G.; Dreyfus, S.; Justwan, H.; Wood, E.S. Drill-Bit Metamorphism: Recognition and Impact on Show Evaluation. In Proceedings of the SPE Annual Technical Conference and Exhibition, New Orleans, LA, USA, 4–7 October 2009; SPE: San Antonio, TX, USA, 2009; SPE 125218, p. 9.
31. Jones, D.; Davis, C.; Justwan, H.; Wenger, L. Effect of PDC-bit platelets on geochemical data quality and hydrocarbon-systems evaluation. In Proceedings of the 25th IMOG Interlaken, Interlaken, Switzerland, 18–23 September 2011; European Association of Roganic Geochemistry: Montpelier, France; p. 1.


**Disclaimer/Publisher's Note:** The statements, opinions and data contained in all publications are solely those of the individual author(s) and contributor(s) and not of MDPI and/or the editor(s). MDPI and/or the editor(s) disclaim responsibility for any injury to people or property resulting from any ideas, methods, instructions or products referred to in the content.